

Phase separation in a 2-d binary colloidal mixture by quorum sensing activity

Jalim Singh and A. V. Anil Kumar*

School of Physical Sciences, National Institute of Science Education and Research, HBNI, Jatni, Bhubaneswar 752050, India.

(Dated: May 19, 2022)

We present results from the Langevin dynamics simulations of a glassy active-passive mixture of soft-repulsive binary colloidal disks. Activity on the small particles is applied according to the quorum sensing (QS) scheme, developed for this study, in which a small particle will be active for a persistence time if its local nearest neighbours are equal to or greater than a certain threshold value. We start with a passive glassy state of the system and apply activity to the smaller size particles, which shows a non-monotonous continuous glassy character of the active particles with the persistence time of the active force, from its passive limit (zero active force). On the other hand, passive particles phase separate at an intermediate persistence time of the active force, resulting the system into the hexatic-liquid and solid-liquid phases. Thus, our system shows three regimes as active glass, phase separation, and active liquid as the persistence time increases from its smaller values. We show that the solid and hexatic phases consisting of passive large particles are stable due to the smaller momentum transfer from active to passive particles compared to the higher persistence time where the positional and orientational ordering vanishes. Our model is relevant to the active biological systems, where glassy dynamics is present, *e.g.*, bacterial cytoplasm, biological tissues, dense QS bacteria, and in the synthetic smart amorphous glasses.

Introduction—Active (self-propelled) particles consume energy from within the system and drive themselves to a non-equilibrium state [1, 2]. Systems with self-propelled particles are of great interest from the perspective of fundamental physics and they are ubiquitous in nature. Examples of living active matter systems are but not limited to sperm swarming [3], bird-flocking and fish schools [4], biological microswimmers [5], quorum sensing bacteria [6]. Another class of active systems is synthetic active matter, examples include artificial microswimmers [2], active mechanical (micro and nano) robots [7], synthetic quorum sensing systems [8] that are useful for the directed mechanical work, targeted drug delivery, biomarkers, and local density dependent motility. Motile bacteria sense a local concentration of the signaling molecules and themselves (*e.g.*, acyl-homoserine lactones in gram-negative bacteria) to perform virulence, biofilm formation, *etc.*, which is termed as quorum sensing (QS) [9]. Bacteria use the QS to produce, release, and sense the extracellular chemical signals that are called as autoinducer molecules for the cell-cell communication. The number of autoinducer molecules increases as a function of the bacterial cell density: at a cell density threshold these molecules activate gene transcriptions of the bacterial cells.

Several living systems including bacterial cytoplasm, collective cell migration show the fingerprints of glassy dynamics [10, 11]. Glasses are dense amorphous systems, and their one of the hallmarks is a dramatic slowdown of the density relaxations with a minimal change in their structure [12]. The glassy dynamics of the bacterial cytoplasm arises from its crowded (dense) intracellular components, which fluidizes by the metabolic activities of the bacterial cell, showing an active glassy characteristic [10]. Another class of active-glass systems are smart amorphous materials (artificial systems) including phase-

changing materials, self-healing glasses [11]. Experimental study of these active materials is difficult at high density, where passive system shows glassiness. Very recently, Klongvessa *et al.* performed an experiment on the gold colloidal particles that are called as active janus colloids, half coated with platinum at high volume fractions [13]. The authors have concluded that active glass slows down at the smaller activity, whereas its fluidization enhances at high activity, which is a non-monotonous character of the active glassy janus colloids. Simulation studies by Szamel and Berthier [14, 15] also show the non-monotonous character in the (all-)active glassy binary colloidal mixture. Another simulation study of the active-passive binary mixture shows that activity fluidizes the glassy state [16].

Active DNAs in the interphase of a chromosome drive to the segregated domains, consisting of euchromatin and heterochromatin that is from the phase separation of active-passive components [17]. Recently, a study of activity induced phase separation in a monodisperse soft-repulsive active-passive disks by Stenhammer *et al.* [18] shows the presence of segregated active and passive domains, where the compression waves originating from the corona of active particles causes the crystallization of the passive particles. In a soft-repulsive active dumbbells the liquid (or gas) and hexatic phase coexistence is reported by Cugliandolo *et al.* [19]. These studies also show that the motility induced phase separation (MIPS) [20–25] is not true in general, where phase separation occurs at a threshold value of the activity. Thus, it prompts us to study the activity induced phase separation in a dense active-passive mixture. In our study, we simulate a 2D binary colloidal mixture consisting of small and large size particles in its glassy state. The small particles are kept motile depending upon their local nearest neighbours (local density), n_b^{fcs} to replicate the local density dependent

sensing in QS bacteria. Our system could be a model system for the smart amorphous materials, and the quorum sensing in a crowded bacteria. We use three control parameters in our simulations: activity f_a , persistence time τ_p , and the n_b^{fcs} that determines the number density of active particles in our system. Starting from the passive glass, our system shows enhanced glassiness at small τ_p (mixed phase), which first phase separate into hexatic-liquid and then to the solid-liquid at the intermediate τ_p ; solid and hexatic phases in the phase separation regime are formed only from the large (passive) particles. Further increasing τ_p at activity f_a fluidizes both species of the particles that are mixed together.

Recently, it has been argued that a two dimensional solid, consisting of hard disks [26] and soft disks [27], melts in two steps: a solid to hexatic continuous transition, and hexatic to a liquid first order transition. This melting occurs if the volume fraction (or density) is decreased at a constant temperature, and agrees with the Kosterlitz, Thouless, Halperin, Nelson, and Young (KTHNY) two-step framework [28–30]. Solid phase is characterized by the quasi-long-range positional order and proper long-range orientational order, whereas hexatic phase is characterized by quasi-long range orientational order and short-range positional order. Our system also shows the hexatic order and the positional order in the phase separation regime.

Modeling—We simulate a 50:50 mixture consisting of 1000 binary colloidal disks of the size ratio 1:1.4 that prevents crystallization, and is a well-known glass-forming system [31, 32]. The interactions between the particles are modeled by a purely repulsive Lennard-Jones potential [33], $V(r_{ij}) = 4\epsilon[(\sigma_{\alpha\beta}/r_{ij})^{12} - (\sigma_{\alpha\beta}/r_{ij})^6 + \frac{1}{4}]$; cut-off for the interaction potential is used as $r_c^{\alpha\beta} = 2^{1/6}\sigma_{\alpha\beta}$. Here $(\alpha, \beta) \in (A, B)$, $\epsilon = 1.0$, $\sigma_{AA} = 1.4\sigma_{BB}$, $\sigma_{AB} = 1.2\sigma_{BB}$, and $\sigma_{BB} = 1.0$. The system is simulated at the area fraction $\phi = 0.628$ that is calculated as $\phi = \pi\rho(\sigma_{AA}^2 + \sigma_{BB}^2)/8$. The equations of motion of the particles are of stochastic type, *i.e.*, Langevin equations

$$m_i \ddot{\mathbf{r}}_i = -\gamma \dot{\mathbf{r}}_i + \sum_{ij} \mathbf{F}_{ij} + \mathbf{F}_i^a + \sqrt{2k_B T} \gamma \boldsymbol{\eta}_i, \quad (1)$$

where γ is the friction coefficient, $\mathbf{F}_{ij} = -\nabla V(r_{ij})$, T is the thermal noise temperature, \mathbf{F}_i^a is the active force of magnitude f_a , and $\boldsymbol{\eta}_i$ is the random gaussian noise with zero mean and unit variance as $\langle \boldsymbol{\eta}_i \rangle = 0$ and $\langle \eta_{i\alpha}(t) \eta_{j\beta}(t') \rangle = 2k_B T \gamma \delta_{ij} \delta_{\alpha\beta} \delta(t - t')$. We apply active force to the small particles using a scheme to replicate the QS dependent motility, which is discussed in detail in the Supplementary Material (SM). We calculate number of nearest neighbours, N_{nn} of each B particle within the first coordination shell (FCS) of $g_B(r)$ (see SM). If the N_{nn} of a particle are equal to or greater than a certain threshold value, *e.g.*, $N_{nn} = 4$ it becomes active.

Results and discussions—Fig. 1 shows a phase diagram of the binary active-passive mixture in $\tau_p - f_a$ plane,

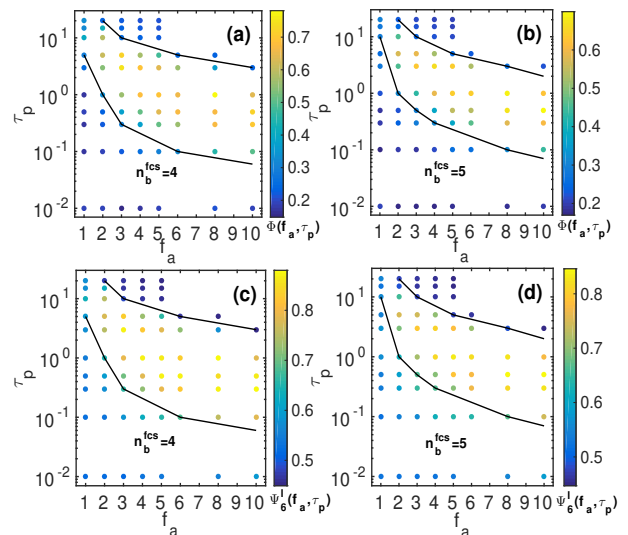


Figure 1. Phase diagram of 2D active-passive binary mixture in $\tau_p - f_a$ plane. Order parameter of phase separation, $\Phi(f_a, \tau_p)$ (a) $n_b^{fcs} = 4$ and (b) $n_b^{fcs} = 5$. Average hexatic order parameter for large (A) particles, *i.e.*, $\Psi_6^l(f_a, \tau_p)$ (c) $n_b^{fcs} = 4$ and (d) $n_b^{fcs} = 5$. Black lines are corresponding to a critical value of $\Phi_c(f_a, \tau_p) = 0.3$.

which has three control parameters, *i.e.*, active force f_a , persistence time τ_p , and number density of active B particles, ρ_{ab} that is controlled by the quorum sensing scheme; the range of $\rho_{ab} = 0.256 - 0.27$ for $n_b^{fcs} = 4$ and $\rho_{ab} = 0.2 - 0.265$ for $n_b^{fcs} = 5$. The shift in the range of ρ_{ab} towards a smaller value for $n_b^{fcs} = 5$ is natural, as the number of B particles with $N_{nn} = 5$ or greater decrease compare to the $n_b^{fcs} = 4$. The phase diagram at $n_b^{fcs} = 4$ (see Fig. 1(a)&(c)) shows three regimes separated by the two transition lines: bottom transition line (BTL) separates active colloidal glass and the phase separation. One of the configuration of active colloidal glass ($\tau_p = 0.1$ and $f_a = 3$) is shown in the Fig. 2(a), where few of the particles show orientational order parameter, $\psi_6^j \approx 1$ [34]. At one of the transition point of the BTL ($\tau_p = 0.3$ and $f_a = 3$), the configuration of Fig. 2(b) shows a growth in the hexatic order comprising A (passive) particles, whereas the B (active) particles start fluidizing. The top transition line (TTL) of the phase diagram separates the phase separation region and the liquid phase of the mixed active-passive particles (see Fig. 2(d)). Between these two transition lines, there exists a solid phase, consisting of only A particles, separated by the fluid phase (see Fig. 2(c)), corresponding to an extent of the phase separation in the system. The RDFs of the solid phase consisting of only A particles are displayed in Fig. 4(c)&(d) that are fitted with the power law. Further, the fluid phase in the phase separated region shows liquid-gas coexistence (see RDF in SM). The scenario is similar for the $n_b^{fcs} = 5$ (see Fig. 1(b)&(d)), except that

the shift in the BTL towards higher persistence time τ_p and, a region of active glass at $\tau_p = 15, 20$ of $f_a = 1$.

The active glass (below BTL), active liquid (above TTL), and the phase separation (between BTL and TTL) regimes are identified by two order parameters: one is the phase separation order parameter $\Phi(f_a, \tau_p)$ and another is the average hexatic orientational order parameter of the large particles, $\Psi_6^l(f_a, \tau_p)$. To compute the $\Phi(f_a, \tau_p)$, we divide the whole 2D simulation box into the number of square cells of equal area, $N_{cell} = 7 \times 7$, which can be obtained by choosing an arbitrary value of cell length (along each spatial direction of the box length, L), $l_c = 6$ for this study. This value of the cell length is chosen such that each cell contains enough number of A and B particles, which subsequently makes the smoother values of the phase separation order parameter. Thus, we calculate phase separation order parameter [35] for the binary colloidal mixture as

$$\Phi(f_a, \tau_p) = \frac{1}{N_{cell}} \left\langle \sum_{i=1}^{N_{cell}} \frac{|n_A^i - n_B^i|}{(n_A^i + n_B^i)} \right\rangle, \quad (2)$$

where N_{cell} is the number of cells in the system, and n_A^i, n_B^i are the number of A and B particles in an i th cell, respectively. The onset of the phase separation is considered at a critical value of the $\Phi(f_a, \tau_p)$ as $\Phi_c(f_a, \tau_p) = 0.30$ in this study; the values of $\Phi_c(f_a, \tau_p)$ are shown by the BTL and TTL in the phase diagram (see Fig. 1) at each f_a along the line of persistence time $\tau_p = 0.01 - 20$. To obtain the $\Phi_c(f_a, \tau_p)$ at each activity f_a , we computed the probability distribution of disparity in the number of A and B particles in each cell, which is calculated as $\chi = (n_A^i - n_B^i)/(n_A^i + n_B^i)$ over the steady states of the system at each activity along the line of τ_p [35]. Then, we compute the distribution of χ as $P(\chi)$, which is shown in the Fig. 3(a)&(b). Fig. 3(a) shows that $P(\chi)$ has a single peak around $\chi = 0$ at $\tau_p = 0.01$, its height start decreasing as the persistence time increases at $f_a = 3$.

The decrement in the peak height of the $P(\chi)$ is accompanied with its broadening and the splitting into two peaks, which is started from $\tau_p = 0.3$ and $f_a = 3$ (one of the transition points of BTL) of $n_b^{fcs} = 4$ (see Fig. 3(a)). This is a clear signature of the disparity in the number of A and B particles in a square cell. As the τ_p increases further, both peaks in Fig. 3(a) grow, an extent to the phase separation is shown (for example) at $\tau_p = 3$ and 5 of $f_a = 3$, where both peaks in $P(\chi)$ separate completely and the height also increases. Above TTL, both peaks of $P(\chi)$ merge again, resulting into a single peak that exhibits the mixing of active and passive particles. A visualization of an extent to the phase separation is shown in Fig. 2(c) at $\tau_p = 3$ and $f_a = 3$ using their single particle coordinates with the color according to the ψ_6^j defined below. For $n_b^{fcs} = 5$ (see Fig. 3(b)), the qualitative nature of the system is similar, though the extent of phase separation is reduced because of the smaller ρ_{ab} .

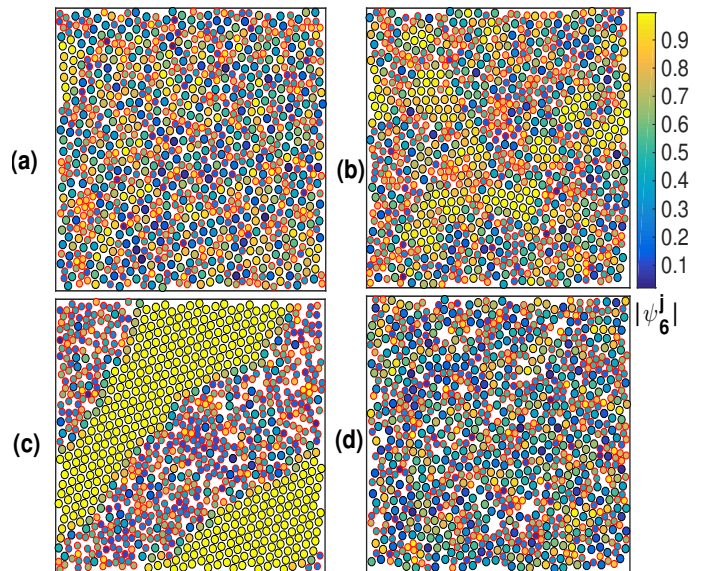


Figure 2. Steady state configurations of the active-passive mixture at $n_b^{fcs} = 4$, $f_a = 3.0$, and persistence time (a) $\tau_p = 0.1$, (b) $\tau_p = 0.3$, (c) $\tau_p = 3.0$, (d) $\tau_p = 15.0$. Color bar is according to the hexatic orientational order parameter ψ_6^j .

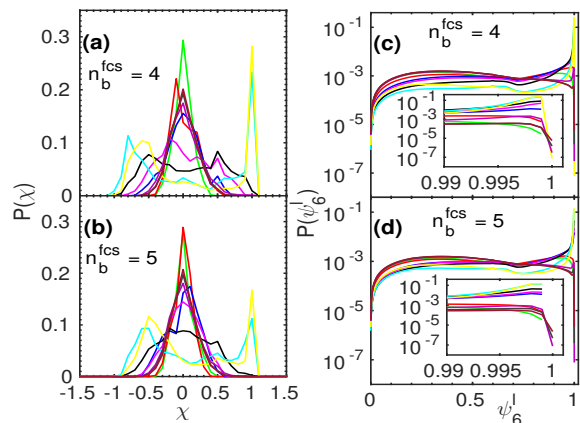


Figure 3. Probability distribution of phase separation order parameter, $P(\chi)$ and local hexatic orientational order, $P(\psi_6^j)$ at $f_a = 3.0$ along the line of persistence times $\tau_p = 0.01 - 20.0$ at $n_b^{fcs} = 4$ (a,c) and $n_b^{fcs} = 5$ (b,d). The colors are according to the legend of Fig. 5.

The single particle hexatic orientational order parameter is calculated as $\psi_6^j = (1/N_{nn}^j) \sum_{k=1}^{N_{nn}^j} \exp(i6\theta_{jk})$, where N_{nn}^j are the nearest neighbours of a particle j , and θ_{jk} is the angle between the radius vector \mathbf{r}_{jk} and the reference axis (x-axis) [31, 36]. We computed the N_{nn}^j of each particle according to the criterion of the distance at the first coordination shell of $g(r)$ of the corresponding type of particles, *e.g.*, we have shown $g_B(r)$ in the Fig. S2 of SM. The average absolute value of the hexatic orientational order parameter is calculated as $\Psi_6 = (1/N_\alpha) \sum_{j=1}^{N_\alpha} |\psi_6^j|$, where N_α is the number of particles of type $\alpha \in (A, B)$. Thus, we computed

$P(\psi_6)$, Ψ_6 , and the hexatic orientational correlation, $g_6(r) = \langle \psi_6^j \psi_6^{k*} \rangle_{|\mathbf{r}_j - \mathbf{r}_k| = r} / \langle |\psi_6^j|^2 \rangle$ to examine the ordering in the system. The average $\Psi_6^l = 0.87$ at $\tau_p = 3$, $f_a = 3$ for $n_b^{fcs} = 4$ (see the phase diagram of Fig. 1(c)), which is a highest value of Ψ_6^l at $f_a = 3$ along the line of $\tau_p = 0.01 - 20$. From the phase diagram, it is evident that the growth of Φ is highly correlated with the Ψ_6^l , except at the higher τ_p , where the system is in mixed state that lowers the Φ similar to the active glass regime. However, the Ψ_6^l above the TTL decreases compare to below the BTL because activity reduces the local hexatic order that can be visualized by comparing Fig. 2(a-d). The distribution of orientational order parameter for A (large) particles, $P(\Psi_6^l)$ is shown in Fig. 3(c) for $n_b^{fcs} = 4$. The $P(\Psi_6^l)$ shows an increment in the orientational order as the peak near $\Psi_6^l = 1$ grows with τ_p that is maximum at $\tau_p = 3$ and 5 of $f_a = 3$. From $\tau_p = 10$, the peak near $\Psi_6^l = 1$ again start decreasing, and becomes even smaller than the $\tau_p = 0.01$. This is because at high τ_p (near the TTL), the solid phase start melting to the liquid, which is also supported by the merging of double peak in a single peak in the $P(\chi)$ (see Fig. 3(a)).

A plot of $g_6(r)$ and its fitting is displayed in Fig. 4(a) and Fig. 4(b) corresponding to $n_b^{fcs} = 4$ and $n_b^{fcs} = 5$, respectively. Fig. 4(a) shows that the $g_6^{AA}(r)$ is fitted with the power law $g_6^{AA}(r) \propto r^{\eta_6}$ with an exponent η_6 that grows continuously on increasing the τ_p from its passive limit till the solid phase consisting of large particles is formed; the exponent $\eta_6 = -3.2$ for the passive system (see Fig. S1(d) of SM). The η_6 increases, and reaches a value near $\eta = -0.01$ at the $\tau_p = 3.0$ and 5.0, which is larger than $-1/4$ for a continuous KTHNY transition to the hexatic phase. The $g_6^{AA}(r)$ decays very slow at the $\tau_p = 3.0$ and 5.0 even at longer distances, which manifests the proper long-range orientational order in A particles. Again, increasing the τ_p of the active force near the TTL, *viz.* $\tau_p = 10.0$ onwards of $f_a = 3.0$, the solid phase melts and the hexatic order reappear. This causes the faster decay of the $g_6^{AA}(r)$, which is shown in the Fig. 4(a) and the exponent η_6 again decreases to -2.89 that shows the hexatic orientational order in A particles. For $n_b^{fcs} = 5$, the qualitative nature of the $g_6^{AA}(r)$ is similar, though it differs quantitatively, because the number density of the active B particles is smaller that causes less phase separation.

We calculate the RDF of AA particles *i.e.*, $g_{AA}(r)$ to examine the positional order in the system. Fig. 4(c) and Fig. 4(d) show $g_{AA}(r)$ and its fitting for $n_b^{fcs} = 4$ and 5, respectively; more RDFs can be found in the SM. The $g_{AA}(r)$ is fitted with the power law of the form $g_{AA}(r) \propto r^\eta$ at the $\tau_p = 3.0$ and 5.0; the obtained exponents are $\eta = -1.42$ and -1.31 that are far smaller than the stability limit of the solid phase, *i.e.*, $-1/3$ in the KTHNY continuous transition. The power law decay of the $g_{AA}(r)$ shows the quasi-long range positional order

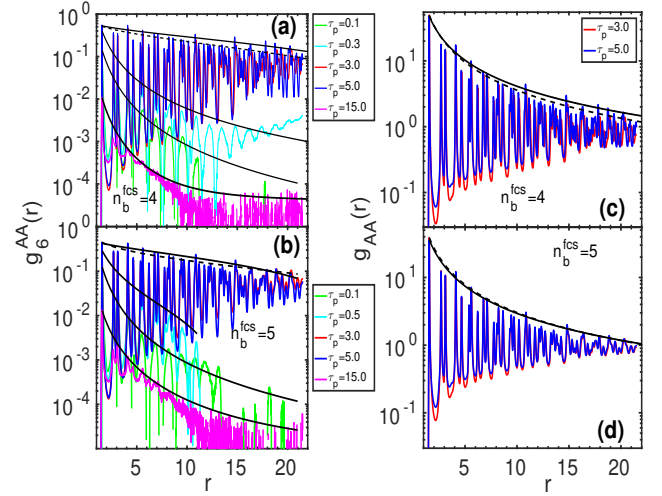


Figure 4. Hexatic order correlations in (a) and (c) for $n_b^{fcs} = 4$ and 5; RDF in (b) and (d) for $n_b^{fcs} = 4$ and 5. The fitting of $g_6^{AA}(r)$ in (a) shows a power law $g_6^{AA}(r) \propto r^{\eta_6}$ with the exponents $\eta_6 = -2.78, -2.26, -0.035, -0.014, -2.89$ at $\tau_p = 0.1, 0.3, 3.0, 5.0, 15.0$, respectively. The fitting of $g_6^{AA}(r)$ in (b) shows the power law with exponents $\eta_6 = -2.68, -1.53, -0.15, -0.19, -2.53$ at $\tau_p = 0.1, 0.5, 3.0, 5.0, 15.0$, respectively. In (c) and (d) RDF of A particles shows (quasi)-long-range positional order.

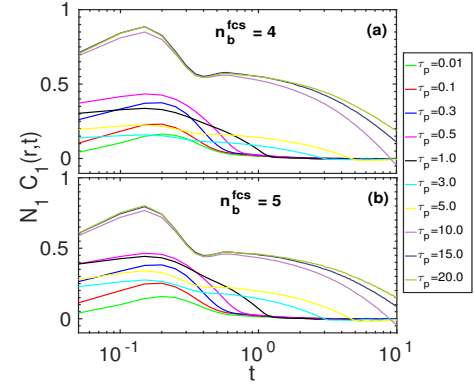


Figure 5. Velocity cross correlations ($B - A$) within the first coordination shell at the persistence times $\tau_p = 0.01 - 20.0$ at $f_a = 3.0$.

in the A (passive) particles. Thus, the passive particles consisting of A particles are in solid phase at $\tau_p = 3.0$ and 5.0 of $f_a = 3.0$ that melts and hexatic orientational order reappear at the τ_p near the TTL. The extent of the phase separation in the system is coincides with the phase separation of the solid phase consisting of only passive A particles: it is shown in Fig. 2(c) for the visualization. On the other hand, height of the peaks in the $g_{BB}(r)$ (see SM) decreases with r and oscillate around $g_{BB}(r) = 2.0$ till $r = 4.0$. It goes below 1.0 at longer distances, showing the liquid-gas phase coexistence for the active particles, which is separated with the solid phase consisting of only A particles.

The QS active particles inject energy into the system that induces the transition from the active glass to the solid-liquid to active liquid phases. We calculate velocity cross correlations [37, 38] from B to A particles to examine the momentum transfer between them, which is defined as

$$C_n(r, t) = \frac{1}{N_n} \frac{\langle \mathbf{v}_i(0) \cdot \mathbf{v}_j(t) \rangle_n}{\langle v_i^2(0) \rangle}, \quad (3)$$

where N_n are the number of particles in the n^{th} coordination shell. The $N_1 C_1(r, t)$ is displayed in the Fig. 5 at $f_a = 3$ along the line of persistence time. The momentum transfer from B to A particles is small at smaller τ_p that increases with it up to $\tau_p = 0.5$. This is because the activity is insufficient to break the cages of the particles at small τ_p and the system remains in the (active) glassy state. The transfer of momentum from B to A particles decreases at $\tau_p = 1.0$ and 3.0 , it start increasing again from $\tau_p = 5.0$, though it is less than $\tau_p = 0.3$. At this intermediate τ_p , activity fluidizes the glassy B particles, whereas the A particles, which are passive in nature start separating, resulting into the (quasi-) long-range positional and orientational ordering. At intermediate τ_p , activity does not diminish the ordering of the A particles, instead enhance the phase separation in the system. Fig. 5 shows that the momentum transfer from B to A particles is pronounced at $\tau_p = 10, 15, 20$ as the peak heights of $N_1 C_1(r, t)$ shoots up again because the τ_p is large enough to destroy the ordering of the A (passive) particles. Thus, the resulting phase appears as an active liquid that shows the mixing of A and B particles.

Conclusion—We have developed a model system for the dense active systems, where activity will be introduced by a local density dependent quorum sensing scheme. By applying activity to the small particles in the binary mixture, the system phase separate at the intermediate persistence time of the activity. Thus, the active-passive binary mixture shows a continuous growth of hexatic order consisting of passive (large) particles from its passive glassy state on increasing persistence time at a constant activity, till the formation of solid phase. Further, increasing the persistence time, the positional order vanishes and the hexatic order reappears that reduces with the persistence time. Finally, we have found that the stability in the solid phase is due to the least momentum transfer from active to the passive particles in the phase separation regime.

The authors acknowledge the financial support from Department of Atomic Energy, India through the 12th plan project(12-R&D-NIS-5.02-0100).

* anil@niser.ac.in

[1] S. Ramaswamy, Ann. Rev. Condens. Matter Phys. **1**, 323 (2010).

- [2] C. Bechinger, R. D. Leonardo, H. Löwen, C. Reichhardt, G. Volpe, and G. Volpe, Rev. Mod. Phys. **88**, 045006 (2016).
- [3] A. Guidobaldi, Y. Jeyaram, I. Berdakin, V. V. Moshchalkov, C. A. Condat, V. I. Marconi, L. Giojalas, and A. V. Silhanek, Phys. Rev. E **89**, 032720 (2014).
- [4] J. Krause and G. D. Ruxton, *Living in Groups* (Oxford University Press, Oxford, 2002).
- [5] H. C. Berg and L. Turner, Nature **278**, 349 (1979).
- [6] K. Papenfort and B. L. Bassler, Nat. Rev. Microbiol **14**, 576 (2016).
- [7] J. Li, B. E.-F. de Ávila, W. Gao, L. Zhang, and J. Wang, Sci. Rep. **2**, eaam6431 (2017).
- [8] T. Bäuerle, A. Fischer, T. Speck, and C. Bechinger, Nat. Comm. **9**, 3232 (2018).
- [9] M. Whiteley, S. P. Diggle, and E. P. Greenberg, Nature **551**, 313 (2017).
- [10] B. R. Parry, I. V. Surovtsev, M. T. Cabeen, C. S. O’Hern, E. R. Dufresne, and C. Jacobs-Wagner, Cell **156**, 183 (2014).
- [11] L. M. C. Janssen, J. Phys.: Condens. Matter **31**, 503002 (2019).
- [12] L. Berthier, G. Biroli, J. Bouchaud, L. Cipelletti, and W. Saarloos, eds., *Dynamical Heterogeneities in Glasses, Colloids and Granular Media* (Oxford University Press, New York, 2011).
- [13] N. Klöngvessa, F. Ginot, C. Ybert, C. Cottin-Bizonne, and M. Leocmach, “Nonmonotonic behavior in the dense assemblies of active colloids,” [1904.02055](https://arxiv.org/abs/1904.02055) (2019).
- [14] L. Berthier, E. Flenner, and G. Szamel, New J. Phys. **19**, 125006 (2017).
- [15] L. Berthier, E. Flenner, and G. Szamel, J. Chem. Phys. **150**, 200901 (2019).
- [16] R. Mandal, P. J. Bhuyan, M. Rao, and C. Dasgupta, Soft Matter **12**, 6268 (2016).
- [17] A. R. Strom, A. V. Emelyanov, M. Mir, D. V. Fyodorov, X. Darzacq, and G. H. Karpen, Nature **547**, 241 (2017).
- [18] J. Stenhammar, R. Wittkowski, D. Marenduzzo, and M. E. Cates, Phys. Rev. Lett. **114**, 018301 (2015).
- [19] L. F. Cugliandolo, P. Digregorio, G. Gonnella, and A. Suma, Phys. Rev. Lett. **119**, 268002 (2017).
- [20] F. Peruani, A. Deutsch, and M. Bär, Phys. Rev. E **74**, 030904(R) (2006).
- [21] J. Tailleur and M. E. Cates, Phys. Rev. Lett. **100**, 218103 (2008).
- [22] A. B. Samuel R. McCandlish and M. F. Hagan, Soft Matter **8**, 2527 (2012).
- [23] A. Suma, G. Gonnella, D. Marenduzzo, and E. Orlandini, Euro. Phys. Lett. **108**, 56004 (2014).
- [24] M. E. Cates and J. Tailleur, Ann. Rev. Condens. Matter Phys. **6**, 219 (2015).
- [25] D. Geyer, D. Martin, J. Tailleur, and D. Bartolo, Phys. Rev. X **9**, 031043 (2019).
- [26] E. P. Bernard and W. Krauth, Phys. Rev. Lett. **107**, 155704 (2011).
- [27] S. C. Kapfer and W. Krauth, Phys. Rev. Lett. **114**, 035702 (2015).
- [28] J. M. Kosterlitz and D. J. Thouless, J. Phys. C: Solid State Physics **6**, 1181 (1973).
- [29] B. I. Halperin and D. R. Nelson, Phys. Rev. Lett. **41**, 121 (1978).
- [30] A. P. Young, Phys. Rev. B **19**, 1855 (1979).
- [31] T. Hamanaka and A. Onuki, Phys. Rev. E **74**, 011506

- (2006).
- [32] T. Kawasaki and H. Tanaka, *J. Phys.: Condens. Matter* **23**, 194121 (2011).
 - [33] J. P. Hansen and I. R. McDonald, *Theory of Simple Liquids* (Academic Press, London, 2006).
 - [34] Glassy state of the active system is characterized using the traditional density relaxations that show stretched-exponential decay (see SM).
 - [35] S. S. N. Chari, C. Dasgupta, and P. K. Maiti, *Soft Matter* **15**, 7275 (2019).
 - [36] K. Binder, S. Sengupta, and P. Nielaba, *J. Phys.: Condens. Matter* **14**, 2323 (2002).
 - [37] U. Balucani, R. Vallauri, and C. S. Murthy, *Phys. Lett.* **84A**, 133 (1981).
 - [38] A. Verdaguer and J. A. Padró, *J. Chem. Phys.* **114**, 2738 (2001).
 - [39] E. Vanden-Eijnden and G. Ciccotti, *Chem. Phys. Lett.* **429**, 310 (2006).

Supplemental Materials:: Phase separation in a 2-d binary colloidal mixture by quorum sensing activity

SYSTEM AND SIMULATION DETAILS

The motivation to use the binary mixture of two different sizes of particles with size ratio $\sigma_{AA}/\sigma_{BB} = 1.4$ is that it has sufficient frustration to form a glassy state at low temperatures [31, 32]. The simulation parameters of the system are used as $\epsilon = 1.0$, $\sigma_{AA} = 1.4 \sigma_{BB}$, $\sigma_{AB} = 1.2 \sigma_{BB}$ and the distances are measured in the unit of $\sigma_{BB} = 1.0$. We simulate 1000 total number of particles, where $N_A = 500$ and $N_B = 500$ for the 50:50 mixture. The Langevin's equations of motion

$$m_i \dot{\mathbf{r}}_i = -\gamma \dot{\mathbf{r}}_i + \sum_{ij} \mathbf{F}_{ij} + \mathbf{F}_i^a + \sqrt{2k_B T} \boldsymbol{\eta}_i, \quad (\text{S1})$$

are integrated using a second-order scheme given by Vanden-Eijnden and Ciccotti [39] at a time step $dt = 0.002$ for the active and the corresponding passive system; note that the active system will become passive in the limit of $f_a = 0$ (zero active force). Here, \mathbf{F}_{ij} is the inter-particle interaction force given as $\mathbf{F}_{ij} = -\nabla V(r_{ij})$, and $V(\mathbf{r}_{ij})$ is a purely repulsive and soft Lennard-Jones potential [33]

$$V(\mathbf{r}_{ij}) = 4\epsilon \left[\left(\frac{\sigma_{\alpha\beta}}{r_{ij}} \right)^{12} - \left(\frac{\sigma_{\alpha\beta}}{r_{ij}} \right)^6 + \frac{1}{4} \right] \quad (\text{S2})$$

with a cut-off at $r_c^{\alpha\beta} = 2^{1/6} \sigma_{\alpha\beta}$. We use the friction co-efficient $\gamma = 10.0$ and the area fraction remains constant at $\phi = 0.628$ throughout this study. All the quantities presented here are in the Lennard-Jones (reduced) unit, *i.e.*, reduced density $\rho^* = \rho \sigma^3$, reduced temperature $T^* = k_B T / \epsilon$, reduced time $t^* = (\epsilon / m \sigma^2)^{1/2} t$, reduced force $f^* = f \sigma / \epsilon$ [33]. We prepare the passive binary mixture at $T = 0.01$ after the equilibration of 5×10^7 steps and then stored trajectories up to 2.5×10^6 steps. The equilibrated configuration of the passive system at $T = 0.01$, is used as the initial configuration for the active system. The activity is introduced to the small (B) particles for a finite persistence time according to the local density dependent sensing scheme described below. The active-passive binary mixture, at all activity and persistence time, again runs for the 5×10^7 steps to reach its steady state and then we store the trajectories of the system.

QUORUM SENSING ALGORITHM

Bacteria use quorum sensing (QS) to produce extra-cellular chemical signals that are called as auto-inducer

(AI) molecules for the activation of specific genes transcription. The number AI molecules increases as a function of cell density: at a threshold value of the cell density, these molecules activate the gene transcriptions in the QS bacteria. Thus, the QS bacteria uses the local (neighbouring) density detection algorithm for expressing their genes, virulence, biofilm formation *etc.* [6, 8, 9]. To replicate the behaviour of QS bacteria, we simulate the binary colloidal mixture in two dimensions in which the small particles are being active according to the local density searching algorithm for a finite active force and persistence time. For the range of local density sensing algorithm, we computed the radial distribution function (RDF) of B particles as

$$g_B(r) = \frac{A}{2\pi r \Delta r N N_B} \left\langle \sum_{i=1}^{N_B} \sum_{\substack{j=1 \\ j \neq i}}^{N_B} \delta(r - |\mathbf{r}_j - \mathbf{r}_i|) \right\rangle \quad (\text{S3})$$

for the passive system at $T = 0.01$ and area fraction $\phi = 0.628$, which is shown in Fig. S2(c). We compute the number of nearest neighbours of each B particle within the radius of $r = 1.825$ (red dashed line in Fig. S2(c)) that is the first coordination shell (FCS) for the B particles. A B particle will be active according to the criterion that if $N_{nn}^i \geq n_b^{fcs}$, where N_{nn}^i is the instantaneous number of nearest neighbours of a B particle within the radius $r = 1.825$. The n_b^{fcs} is a fixed finite value that dictates the number density of active B particles in the system. In this study, we present results from the $n_b^{fcs} = 4$ and 5. At $n_b^{fcs} = 6$, only 10 – 15% of the B particles are active (data not presented in this study, which will be reported elsewhere) and at $n_b^{fcs} = 7$, only 1 – 5 active B particles at $\phi = 0.628$ in 2D. We scan the nearest neighbours of each B particle at each $t = \tau_p$, τ_p is the persistence time of the active force. Thus, the number of active particles in our study are varying and according to the quorum sensing rules using the local neighbour searching algorithm.

ACTIVITY

As discussed in the previous section, QS bacteria becomes active by sensing the local density of their neighbours, if it reaches at its certain threshold value. We apply active force on the B particles according the QS scheme for the finite persistence time τ_p , which ranges as 0.01 – 100.0; results of this study are shown up to $\tau_p = 20.0$ only. The active force \mathbf{F}_a^i on the i^{th} particle is given as $\mathbf{F}_a^i = f_a \zeta_i$, where f_a is a magnitude of the active force and ζ_i is a random direction between -1 and $+1$. Thus the active force for B particles in the system can be given as

$$\langle \zeta_{i\alpha}(t) \zeta_{j\beta}(t') \rangle = \delta_{ij} \delta_{\alpha\beta} f_a^2 \quad (\text{S4})$$

for $|t - t'| \leq \tau_p$ and zero otherwise; $(\alpha, \beta) \in (x, y)$.

CONFIGURATIONS OF THE PASSIVE AND ACTIVE SYSTEM

We have prepared a 2D random initial configuration of the binary colloidal mixture at the area fraction $\phi = 0.628$, which is shown in Fig. S1(a). This random initial configuration is equilibrated at temperature $T = 8.0$ using the Langevin dynamics simulations. The final configuration of the equilibrated system at $T = 8.0$ is used as the initial configuration at $T = 0.01$. The final configuration obtained at $T = 0.01$ is shown in Fig. S1(b). To investigate the local orientational order in the system, we invoke the hexatic order parameter (HOP), which entails the information about orientational ordering in 2D that is defined as

$$\psi_6^j = \frac{1}{N_b^j} \sum_{m=1}^{N_b^j} \exp(i6\theta_j^m), \quad (\text{S5})$$

where N_b^j are the number of nearest neighbours of a particle j , θ_j^m is the angle between the radius vector \mathbf{r}_j^m and the reference axis. The values of the ψ_6^j ranges from 0–1, depending on the θ_j^m ; a perfect trigonal corresponds to the $6\theta_j^m = 2\pi$ that has value $\psi_6^j = 1$, whereas the $\psi_6^j = 0$ corresponds to the random orientational arrangement of six nearest-neighbours of a particle j . We use the cut-off distances 2.085 and 1.825 as the second minima of $g_A(r)$ and $g_B(r)$, respectively for calculating the nearest-neighbours of A and B type particles; $g_B(r)$ is shown in Fig. S2(c). A magnitude of local HOP is calculated as $\Psi_6 = |\psi_6^j|$. The absolute values of ψ_6^j of the random initial configuration (see Fig. S1(a)) of the passive mixture shows that it is a disordered configuration except for few particles, for them it shows local hexatic ordering because the natural number of nearest neighbours of a particle are six in a dense 2D system. The equilibrated final configuration of the passive system at $T = 0.01$ shows a local hexatic ordering of A and B particles that can be seen in Fig. S1(b). We calculate probability distribution $P(\Psi_6)$ of the passive colloidal mixture over the equilibrium configurations at $T = 0.01$ to examine the average local hexatic ordering. The $P(\Psi_6)$ of B particles (see Fig. S1(c)) shows a peak around $\Psi \approx 0.9$, which exhibits an emergence of the local hexatic order. The $P(\Psi_6)$ of A particles shows two peaks, one at $\Psi \approx 0.3$ and other at $\Psi \approx 0.9$, which manifests the smaller orientational order in A particles compare to the B particles. To examine a range of hexatic orientational ordering, we compute hexatic order correlation function $g_6(r)$ defined in Eq. ??, which is shown in Fig. S1(d). The $g_6(r)$ is fitted with the power law of exponents -3.2 and -2.0 for AA and BB particles. The smaller value of the exponent for the B particles compared to A particles means a larger hexatic correlation length compare to A particles. Thus, the passive system shows more hexatic orientational ordering

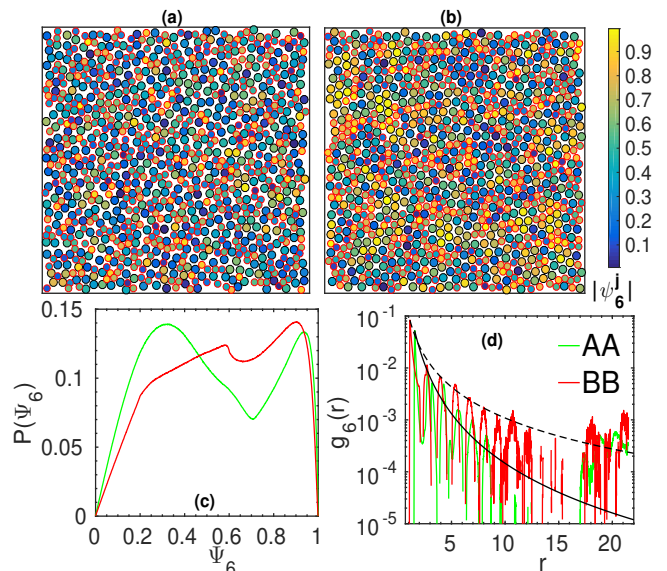


Figure S1. (a) Random initial configuration of the Passive mixture at $\phi = 0.628$, (b) Final configuration of the Passive mixture at $T = 0.01$ and $\phi = 0.628$. The color bar shows single particle hexagonal order parameter $|\psi_6^j|$, (c) Probability distribution Ψ_6 of A (green) and B (red) particles averaged over the equilibrium configurations of the passive system, (d) Hexatic order correlation function $g_6(r)$ fitted with a power law of the form $g_6(r) \propto r^{-\eta_6}$; the exponent $\eta_6 = -3.2$ and -2.0 for AA (solid curve) and BB (dashed curve) particles. Circles with black (red) face represent the large (small) particles in (a) and (b).

for the B particles compared to the A particles.

GLASSY FEATURES OF PASSIVE SYSTEM

The hexatic orientational order found in the absence of positional order at the size ratio 1:1.4 [31], which is termed as the glassy structural order by Kawasaki and Tanaka [32]. Thus, it is tempting to examine the positional order in the system, which can be obtained from the radial distribution function (RDF), $g(r)$ or its Fourier transform, $S(k)$. The RDF of A and B particles can be defined as

$$g_{\alpha\beta}(r) = \frac{A}{2\pi r \Delta r N_\alpha N_\beta} \left\langle \sum_{i=1}^{N_\alpha} \sum_{\substack{j=1 \\ j \neq i}}^{N_\beta} \delta(r - |\mathbf{r}_j - \mathbf{r}_i|) \right\rangle, \quad (\text{S6})$$

where $(\alpha, \beta) \in (A, B)$, A is area of the 2D simulation box, N_A and N_B are number of A and B particles, respectively. The $g(r)$ of AA , BB , and AB is presented in Fig. S2(a), which shows an absence of long-range (or quasi long-range) positional order in the system, however there is a hexatic orientational order as shown in the Fig. S1(c)&(d) above. This confirms that the passive binary colloidal mixture is in its amorphous state.

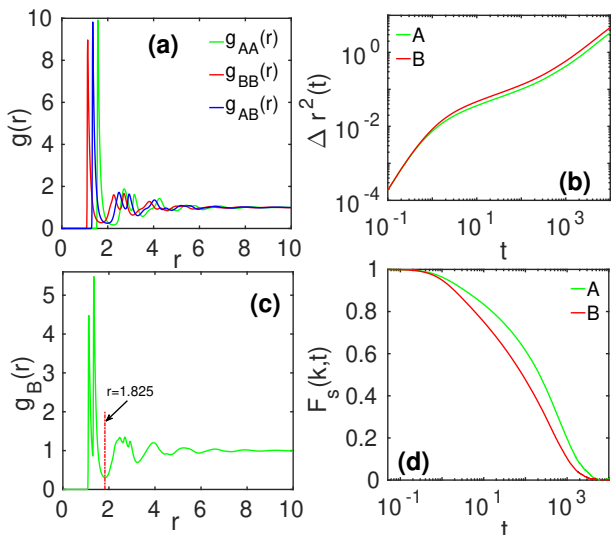


Figure S2. Passive mixture at $T = 0.01$ and the area fraction $\phi = 0.628$: (a) RDFs of the binary colloidal mixture, (b) MSD of A and B particles, (c) Radial distribution of B particles, $g_{B-AB}(r)$, (d) Incoherent intermediate scattering function, $F_s(k, t)$ at wave vectors corresponding to the first peak of static structure factor $S(k)$ of A and B particles, *i.e.*, $k_A = 4.5$ and $k_B = 5.0$.

The $g_{B-AB}(r)$ corresponds to the number of A and B neighbouring particles surrounding a tagged B particle, which we will represent as $g_B(r)$ throughout this paper. The $g_B(r)$ shows two main peaks at $r = 1.125$ and 1.345 : first one corresponds to the BB particles, whereas second one corresponds to the BA particles. Afterwards the minima around $r = 1.825$ (red dashed line in Fig. S2(c)) corresponds to the first co-ordination shell cut-off for $B - AB$ particles, which is used for calculating ψ_6^j and in the quorum sensing scheme.

The structure of the 2D binary mixture shows that the mixture is in an amorphous (glassy) state as described above. The glassy dynamics of the passive binary colloidal mixture is examined using mean-squared displacements (MSD) and the incoherent intermediate scattering function (IISF), which are defined as

$$\Delta r^2(t) = \frac{1}{N} \left\langle \sum_{i=1}^N (\mathbf{r}_i(t) - \mathbf{r}_i(0))^2 \right\rangle \quad (\text{S7})$$

and

$$F_s(k, t) = \frac{1}{N} \left\langle \sum_{j=1}^N \exp(i\mathbf{k} \cdot (\mathbf{r}_j(t) - \mathbf{r}_j(0))) \right\rangle, \quad (\text{S8})$$

where wave vector k corresponds to the first peak of static structure factor of A and B particles. Here, we used $k = 4.5$ and 5.0 for A and B particles, respectively. Fig. S2(b) shows the MSD of A and B particles at $T = 0.01$, which shows a ballistic regime at short times that crossing over to the sub-diffusive regime around $t \approx 1.0$,

becomes diffusive at long times: different regimes in the MSD of A and B particles are identified from the slope $\alpha = \partial \ln \Delta r^2(t) / \partial \ln t$. At short times, $\alpha \approx 2$, in sub-diffusive regime, $0 < \alpha < 1$, while in the diffusive regime $\alpha = 1$. The sub-diffusive regime appears due to the formation of structural cages around a tagged particle by its neighbouring particles [12]. These structural cages cause a slow down in the dynamics, thus the MSD decreases at these time scales. At long times, the particles come out from these structural cages, thus MSD again shoots up and the dynamics becomes diffusive. Although the larger (A) particles are slower than the smaller (B) ones, both size of particles show the sub-diffusive regime at intermediate times (see Fig. S2(b)), which is one of the hallmarks of the glassy dynamics [12]. The structural relaxation of these cages is characterized using the IISF, $F_s(k, t)$ of both size of particles, which also shows slow relaxation for the A particles compare to B particles. The $F_s(k, t)$ examines the relaxation of density fluctuations due to the structural cages of the single particles at a wave vector k . In this passive binary colloidal mixture, $F_s(k, t)$ is fitted using an empirical Kohlrausch-Williams-Watts (KWW) function of the form $f(t)^{KWW} \propto \exp(-(t/\tau)^\beta)$, β is the exponent [12]. The value of the exponent $\beta = 1$ for the exponential density relaxations (liquid state), whereas $0 < \beta < 1$ for the non-exponential relaxations found in slow relaxing systems, *e.g.*, glass-forming liquids, intracellular dynamics, motion in the crowded media, *etc.* For this passive binary mixture, we obtain $\beta = 0.66$ and 0.6 for A and B particles, respectively. These values of β shows the non-exponential relaxation dynamics of the system at $T = 0.01$ and area fraction $\phi = 0.628$, which is a signature of the glassy dynamics in the passive system.

STRUCTURE AND DYNAMICS OF THE ACTIVE SYSTEM

The structure and dynamics of the passive binary disks show characteristics of the glassy systems, which changes with the introduction of activity in the system. Activity in the binary colloidal disks is applied to the small (B) particles with three control parameters, *viz.*, activity f_a , persistence time τ_p , and the number density of active B particles ρ_{ab} . The activity of the B particles increases hexatic orientational ordering in A particles with an increase in the persistence time till the formation of solid phase, near the TTL in the phase diagram of Fig. 1(c)&(d). The solid phase is corresponding a higher value of $\Psi_l(f_a, \tau_p)$ at each activity along the line of τ_p , *e.g.*, $\tau_p = 3.0$ and 5.0 at $f_a = 3.0$. Further increasing the τ_p of the active force, the solid phase consisting of only A particles is first melting into the hexatic phase and then into the liquid phase. Thus, at a longer τ_p , *e.g.*, at $f_a = 3.0$ $\Psi_l(f_a, \tau_p)$ again start decreasing beyond $\tau_p = 5.0$. As dis-

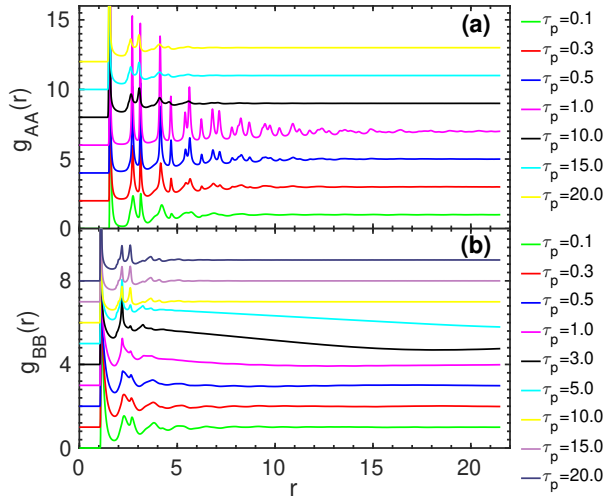


Figure S3. RDF of (a) AA and (b) BB particles at $f_a = 3.0$ for $n_b^{fcs} = 4$. In (a) and (b) plots are shifted by 2.0 and 1.0 along the y -axis for visibility, respectively.

cussed in the main text, the system shows three regimes separated by the two transition lines: active glass, phase separation, and active liquid. These phases are characterized by the hexatic order parameter and the phase separation order parameter in the main text.

It is tempting to look at the structural changes (especially micro-structure) in the binary mixture with the application of activity. Fig. S3(a) shows the RDF of AA particles, *i.e.*, $g_{AA}(r)$ at one of the activity $f_a = 3.0$ in the range of $\tau_p = 0.1$ -20.0 of the phase diagram. The micro-structure of the passive (large) particles becomes rich as the τ_p is increased till the formation of the solid phase (see RDF in main text of Fig. 4(c)). Further increment of the τ_p , reduces the micro-structure rich phase, which is due to the melting of the solid phase first into the hexatic order phase, and then into the liquid phase. However, the RDF of BB particles (Fig. S3(b)) shows the reduction in its micro-structure as the τ_p is increased from the passive limit ($f_a = 0$) of the mixture, till the TTL is reached. Above TTL, the micro-structure in the $g_{BB}(r)$ increases because the mixing of the particles in the active liquid phase. Interestingly, at the persistence times $\tau_p = 3.0$ and 5.0, where the passive particles shows an extent to the phase separation of solid phase, the $g_{BB}(r)$ decays below 1.0, indicating the phase-coexistence of liquid and gas phases; this coexistence region is consisting of small and few large particles.

The dynamics of the active-passive binary soft-repulsive disks is analysed by computing the $F_s(k, t)$ of A and B particles at the wave vectors $k = 4.5$ and 5.0, respectively; the definition of $F_s(k, t)$ is given in the Eq. S8. Fig. S4 shows the $F_s(k, t)$ of A and B particles at the activity $f_a = 3.0$ along the line of persistence time from its smaller value in this study ($\tau_p = 0.01$) to the $\tau_p = 20$ for the local neighbour threshold value $n_b^{fcs} =$

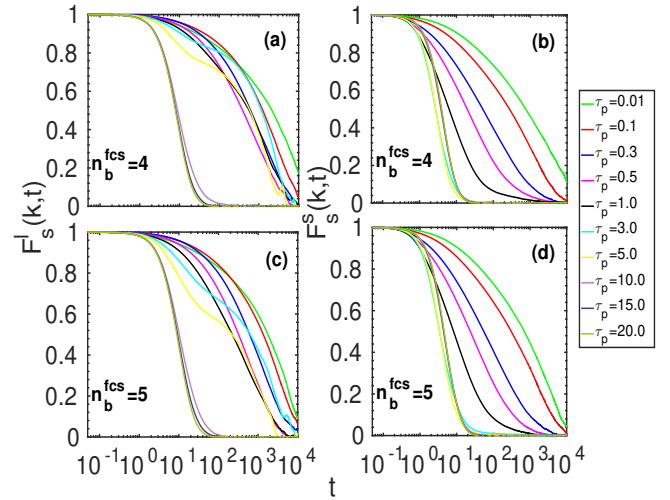


Figure S4. Density relaxation in the active binary colloidal mixture: Incoherent intermediate scattering function $F_s(k, t)$ of (a) large particles for $n_b^{fcs} = 4$, (b) small particles for $n_b^{fcs} = 4$, (c) large particles for $n_b^{fcs} = 5$, and (d) small particles for $n_b^{fcs} = 5$.

4 and 5. On comparing the $F_s(k, t)$ of passive B particles (see Fig. S2(d)) with the active B particles (Fig. S4(b)&(d)), it is evident that the density relaxation in the system becomes slower with the injection of activity at smaller τ_p . Because the $F_s(k, t)$ of passive B particles relax to zero near $t \simeq 5 \times 10^3$, while the $F_s(k, t)$ of B particles in active system is above zero even till the time $t = 10^4$. Interestingly, the $F_s(k, t)$ of A and B particles in active system shows more slowing down for $n_b^{fcs} = 4$ compared to the $n_b^{fcs} = 5$ at smaller τ_p . This slowing down is because the number density of active B particles is more in case of $n_b^{fcs} = 4$, which shows that activity enhances the glassiness in the system at smaller τ_p . At $f_a = 3.0$, as the persistence time of active force increases, $F_s(k, t)$ of B particles shows a faster density relaxations that is due to the activity induced fluidization in the system, thus showing the non-monotonous characteristic of the active dense systems, as reported in a recent experimental [13] and simulation [14, 15] studies of dense active colloidal systems.

On the other hand, the density relaxations of the A particles show a contrasting behavior at the intermediate τ_p , where it phase separate into the hexatic (near the first transition line) and solid phases. The slowing down of the $F_s(k, t)$ at these values of the τ_p is because of the solidification that hinders the movement of the A particles, enormously. At $\tau_p = 3.0$ and 5.0, where it shows the extent of phase separation along the line of persistence time at $f_a = 3.0$, system shows a extreme glassy like density relaxations. This is because all the A particles are not phase separated into the hexatic or solid phases, though, few of the A particles are mixed with the B particles that are in the liquid-gas phase co-existence

region. The mixing of the A and B particles can be visualized in the Fig. 2(g). Thus, our structural analysis

is coinciding with the dynamics of the active-passive 2D binary mixture in its steady state.